Research Article

NMR IN BIOMEDICINE

Received: 29 September 2010, Revised: 29 March 2011, Accepted: 1 April 2011, Published online in Wiley Online Library: 22 July 2011

(wileyonlinelibrary.com) DOI 10.1002/nbm.1737

Accurate noninvasive measurement of cell size and compartment shape anisotropy in yeast cells using double-pulsed field gradient MR

Noam Shemesh[a], Evren Özarslan[b,c], Peter J. Basser[b] and Yoram Cohen[a]*

The accurate characterization of pore morphology is of great interest in a wide range of scientific disciplines. Conventional single-pulsed field gradient (s-PFG) diffusion MR can yield compartmental size and shape only when compartments are coherently ordered using *q*-space approaches that necessitate strong gradients. However, double-PFG (d-PFG) methodology can provide novel microstructural information even when specimens are characterized by polydispersity in size and shape, and even when anisotropic compartments are randomly oriented. In this study, for the first time, we show that angular d-PFG experiments can be used to accurately measure cellular size and shape anisotropy of fixed yeast cells employing relatively weak gradients. The cell size, as measured by light microscopy, was found to be 5.32 ± 0.83 μm, whereas the results from noninvasive angular d-PFG experiments yielded a cell size of 5.46 ± 0.45 μm. Moreover, the low compartment shape anisotropy of the cells could be inferred from experiments conducted at long mixing times. Finally, similar experiments were conducted in a phantom comprising anisotropic compartments that were randomly oriented, showing that angular d-PFG MR provides novel information on compartment eccentricity that could not be accessed using conventional methods. Angular d-PFG methodology seems to be promising for the accurate estimation of compartment size and compartment shape anisotropy in heterogeneous systems in general, and biological cells and tissues in particular.

Keywords: cell size; cell shape; diffusion; NMR; double-PFG; yeast cells; compartment shape anisotropy; microscopic anisotropy

INTRODUCTION

The application of pulsed field gradients (PFGs) can directly sensitize the magnetization arising from NMR-observable nuclei to molecular displacement, thereby enabling the manifestation of diffusion processes in NMR signal decay (1). Endogenous fluids undergoing restricted diffusion within pores and interstices of porous media can be used as excellent reporters on geometrical features of the restricting milieu, enabling the noninvasive characterization of important microstructural information in many opaque systems, such as neuronal tissues (2), isolated cells (3), porous materials (4) and even rocks (5).

Conventional single-PFG (s-PFG) diffusion MR methods employ a single pair of diffusion gradient vectors **G** with duration δ, which are separated by a diffusion period Δ. The important quantity characterizing the diffusion weighting is the wavevector **q**, where $\mathbf{q}=(2\pi)^{-1}\gamma\delta\mathbf{G}$. Conventional s-PFG approaches are useful for obtaining compartment size, especially when monodisperse pores are coherently organized, using the diffusion–diffraction phenomenon (6). When monodisperse pores are anisotropic and coherently placed, the diffusion–diffraction patterns are also extremely sensitive to compartment orientation, thus offering information on the anisotropy of the coherently organized compartments (7). Indeed, diffusion–diffraction experiments have been conducted on various systems, including red blood cells (8,9), narrowly distributed emulsions (10) and even single crystals using electron spin resonance (11). However, these diffusion–diffraction patterns vanish in more heterogeneous specimens characterized by size polydispersity and/or orientation distributions. In such cases, the *q*-space approach (12,13) can be used to estimate compartment sizes. The *q*-space approach entails the sampling of the normalized signal decay $E(q)$ up to high q values, followed by Fourier transformation of the data. The resulting displacement probability distribution functions (PDFs) can be used to estimate the displacement profile in a given component (14). Although the utility of size contrast has been shown in the past in many applications (15–18), recent *ex vivo* *q*-space imaging studies of the spinal cord, employing very high q values and using extremely strong

* *Correspondence to: Y. Cohen, School of Chemistry, The Raymond and Beverly Sackler Faculty of Exact Sciences, Tel Aviv University, Ramat Aviv, Tel Aviv 69978, Israel.*
E-mail: ycohen@post.tau.ac.il

a *N. Shemesh, Y. Cohen*
School of Chemistry, The Raymond and Beverly Sackler Faculty of Exact Sciences, Tel Aviv University, Tel Aviv, Israel

b *E. Özarslan, P. J. Basser*
Section on Tissue Biophysics and Biomimetics, PPITS, NICHD, National Institutes of Health, Bethesda, MD, USA

c *E. Özarslan*
Center for Neuroscience and Regenerative Medicine, USUHS, Bethesda, MD, USA

Abbreviations used: *d-PFG, double-pulsed field gradient; EA, ensemble anisotropy; PDF, probability distribution function; PFG, pulsed field gradient; s-PFG, single-pulsed field gradient; μA, microscopic anisotropy.*

NMR IN BIOMEDICINE

gradients, provided striking evidence suggesting that size contrast can yield 'virtual histology' (19,20). However, these striking results were obtained using extremely strong gradient pulses. In addition, relatively many q values need to be collected, thus rendering the methodology rather demanding.

Diffusion tensor imaging (2), which is conducted at lower q values, can be used to infer ensemble anisotropy (EA) when anisotropic compartments are coherently organized; indeed, diffusion tensor imaging has been used with great success to depict white matter microstructure and to perform fiber tracking in the central nervous system (21). However, another significant drawback of s-PFG methodologies is that they fail to accurately depict compartment anisotropy when eccentric compartments are randomly oriented, as the local diffusion directors are completely averaged within the excited volume, creating macroscopic isotropy.

The double-PFG (d-PFG) methodology is emerging as a novel means to overcome these inherent limitations of s-PFG NMR. The d-PFG sequence (22) is an extension of s-PFG, employing an additional pair of diffusion sensitizing gradients. The d-PFG sequence therefore spans a large parameter space, including the gradient vectors $\mathbf{G_1}$ and $\mathbf{G_2}$, their respective durations δ_1 and δ_2, and the diffusion periods spanned by each gradient pair, namely Δ_1 and Δ_2 (Fig. 1A). Another important parameter unique to d-PFG MR is the duration between the two diffusion periods, namely the mixing time (t_m), which can either have a finite value (Fig. 1A) or can be set to zero (Fig. 1B). Early d-PFG work focused on comparing the signal decay up to high q values when $\mathbf{G_1}$ and $\mathbf{G_2}$ were either parallel or perpendicular, thus offering a glance towards the eccentricity of compartments, such as yeast cells (22,23), liquid crystals (24) and even gray matter and spinal cord in MRI (25,26); other early d-PFG experiments focused on different acquisition schemes, such as two-dimensional diffusion–diffusion correlation approaches (27,28).

Two unique features of d-PFG, which have no parallel or analogs in s-PFG MR, are the angle ψ between the two gradient pairs $\mathbf{G_1}$ and $\mathbf{G_2}$, and the mixing time between diffusion periods, which can be combined to devise the angular d-PFG methodology, first suggested theoretically by Mitra (29). In this methodology,

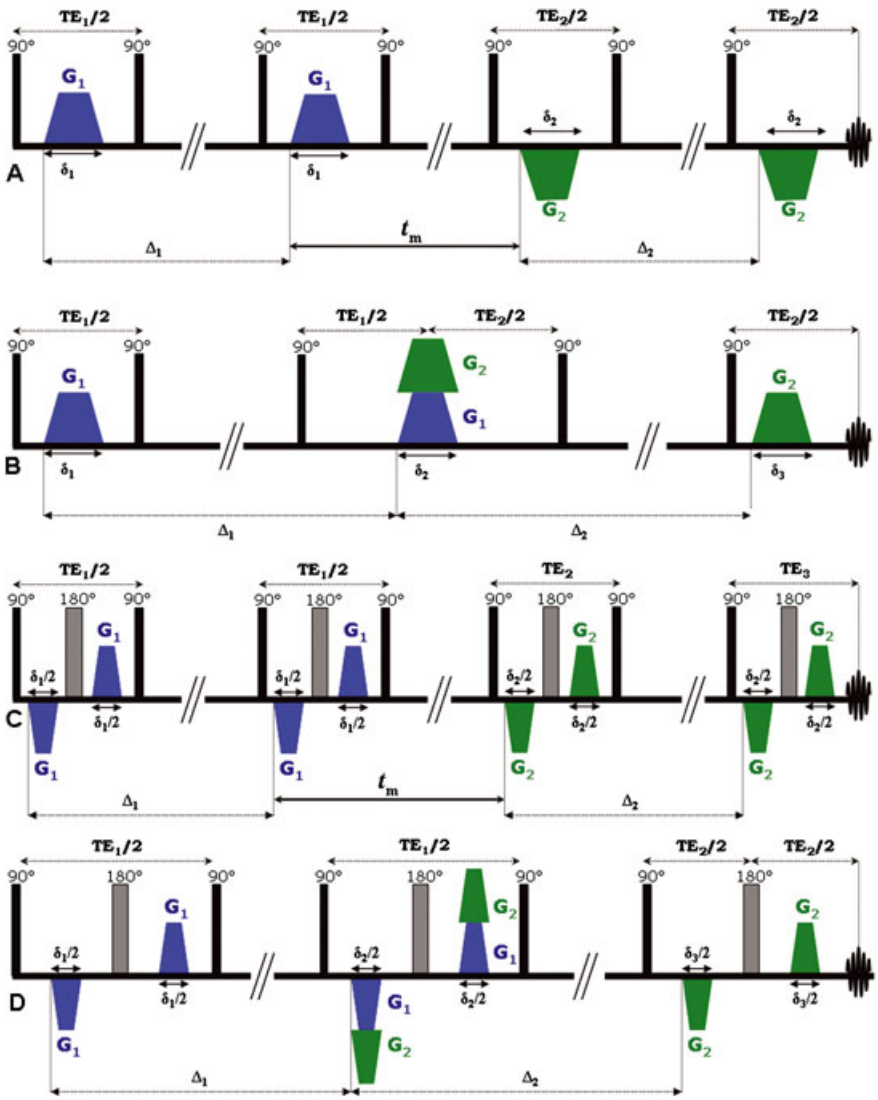

Figure 1. Double-pulsed field gradient (d-PFG) sequences. (A) d-PFG sequence with finite mixing time. Note that, here, $\mathbf{G_1}$ and $\mathbf{G_2}$ are applied in the same directional sense, appearing opposite only because of the pair of 90° radiofrequency pulses between the gradient pairs. (B) d-PFG with zero mixing time. (C) Bipolar d-PFG with finite mixing time. (D) Bipolar d-PFG with zero mixing time. Note that, in the bipolar versions of the d-PFG sequences, the gradient duration is cut in half.

the orientation of $\mathbf{G_1}$ is set in a certain direction, and the orientation of $\mathbf{G_2}$ is varied along the angle ψ (Fig. 2A), whilst keeping the diffusion periods, mixing time and q value for this angular d-PFG experiment constant (in the angular d-PFG experiment, $|\mathbf{q}|=|\mathbf{q}_1|=|\mathbf{q}_2|$, where $\mathbf{q_i}=(2\pi)^{-1}\gamma\delta\mathbf{G_i}$, i.e. the magnitude of the gradients is kept constant and equal). The d-PFG NMR diffusion signal as a function of ψ [hereafter referred to as $E(\psi)$] at a given q value and mixing time was predicted to give rise to angular dependences that offer novel and unique microstructural information. When diffusion is restricted, the angular dependence at $t_m=0$ ms was theoretically predicted to yield a bell-shaped function, from which the pore size could be measured; importantly, these bell-shaped functions were predicted even at low q values (where $2\pi q^* a<1$, where a is the pore dimension), thus offering a novel means for size measurements using mild gradient conditions (29). Considering the potential of compartment size as a useful source of contrast in central nervous system tissues, this could be important, as q-space approaches necessitate very high q values to be reached, i.e. strong gradients need to be implemented (especially in the light of the need to fulfill the short gradient pulse approximation in these approaches).

Recent theoretical advances have provided exact solutions to the diffusion-attenuated MR signal decay for arbitrary timing parameters (30,31) and, subsequently, the theory was extended beyond the $2\pi qa<1$ regime to a general framework for diffusion in NMR (32). Further theoretical progress (33) has suggested that, in addition to compartment size, compartment shape anisotropy can be obtained from d-PFG MR conducted at different mixing times, as different anisotropy mechanisms contribute to the NMR signal at different mixing times (t_m): at short t_m, the d-PFG NMR signal comprises contributions from microscopic anisotropy (μA), compartment shape anisotropy (e.g. the deviation of pores from perfect spheres) and EA (the coherence of packing of anisotropic pores) [for a general treatment of these scenarios, see ref. (33)]. Therefore, the angular d-PFG MR experiment can depict μA at short t_m as long as restricted diffusion occurs, regardless of the compartment anisotropy and organization. By contrast, at long mixing times the effects of μA are decoupled from the signal, and therefore only compartment shape anisotropy dominates the angular dependence, even when anisotropic compartments are randomly oriented (Fig. 2B) or spherical (Fig. 2C). The result is that for spherical compartments (Fig. 2C), which are isotropic, no ψ dependence is predicted resulting in a flat $E(\psi)$ profile at long mixing times, whereas for locally anisotropic pores that are randomly oriented (Fig. 2B), modulated curves that depend solely on compartment eccentricity are predicted (33). Although the modulation in $E(\psi)$ was not predicted to afford refined information on the actual pore shape [for example, cylinders and ellipsoids of the same length and radius would yield similar $E(\psi)$ modulations (33)], the ability to infer the presence of anisotropy on the microscopic scale in the absence of EA implied that angular d-PFG MR could be of importance in characterizing randomly oriented porous media and biological tissue. It should be noted that, when EA exists, it can also be detected in the long-t_m regime.

Although $E(q)$ d-PFG MR measurements using collinear and orthogonal gradient vectors have been performed previously up to high q values, showing that compartment shape could be inferred in yeast cells (23) and in liquid crystals (24), the bell-shaped $E(\psi)$ dependences have been observed experimentally only recently at low q values in both MRS (34) and MRI (35,36) experiments, and the effect of experimental parameters on the bell-shaped functions was studied and accounted for (34), even when a freely diffusing component was included (37). Very recently, the modulated $E(\psi)$ curves at long t_m were experimentally observed for the first time in a controlled system containing a porous medium comprising randomly oriented cylindrical pores (37) using bipolar d-PFG MR sequences (Fig. 1C, D), which are preferable when severe susceptibility effects are present. Other simulations support the idea that angular d-PFG MR can yield novel microstructural information: notably, a tensor approach to angular d-PFG NMR was introduced, where rotationally invariant measures of anisotropy could be extracted (38–41).

In previous studies, controlled specimens in which the ground truth was known *a priori* were used to challenge the theoretical framework in terms of accuracy and robustness of the extracted microstructural information, yielding excellent agreement between experiments and theory at both low (34,37,42) and high (42–44) q values. In the light of the previous findings, we sought to challenge the ability of angular d-PFG to extract microstructural information in a real biological specimen. We therefore performed the angular d-PFG experiments in fixed yeast cells, previously used to study intracellular diffusion coefficients (45), exchange (46) and restricted diffusion (47). The objectives of the present study were to test the viability of angular d-PFG MR as a new means to report on cellular morphology (size and shape) in such realistic specimens noninvasively and, furthermore to challenge the accuracy of the results, to challenge the possibility of doing so using relatively weak gradients and to explore the possibility of contrast between spherical and nonspherical compartments that are randomly oriented, i.e. scenarios in which there is no EA.

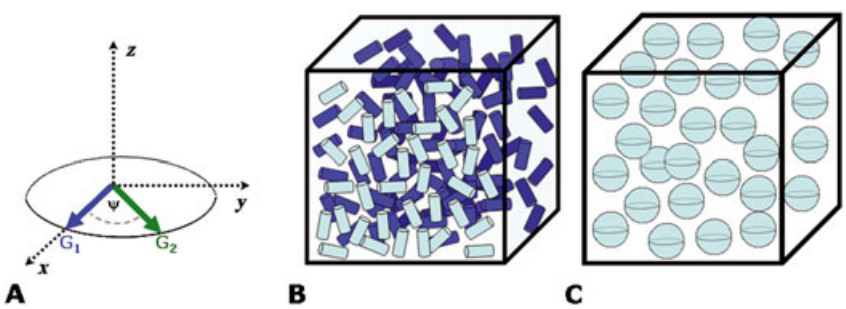

Figure 2. Angular double-pulsed field gradient (d-PFG) methodology and orientation schemes. (A) The angular d-PFG MR methodology involves fixing $\mathbf{G_1}$ in a certain direction, and then performing experiments when only the orientation of $\mathbf{G_2}$ is varied relative to $\mathbf{G_1}$ along the angle ψ. Note that in such experiments, $|\mathbf{G_1}|=|\mathbf{G_2}|$, and therefore the angular d-PFG experiments are conducted at a given q value. (B) A scheme of randomly oriented anisotropic compartments. (C) A scheme of spherical compartments.

NMR IN BIOMEDICINE

MATERIALS AND METHODS

Theory and data analysis

The compartment size measurements were based on the general theoretical framework for diffusion in MR presented in refs. (32) and (33). In this method, a general MR gradient waveform is expressed as a piecewise constant function. Each pulse in the acquisition is represented by a vector whose components are infinite dimensional matrices. The effect of each pulse is then expressed as the exponential of one such matrix. The technique makes it possible to obtain an analytical expression for the diffusion-related MR signal attenuation with relative ease. The analytical expression is exact for piecewise constant gradient waveforms, whereas accurate approximations can be obtained when slowly varying gradients are employed. The reader is referred to ref. (32) for a detailed description of the method, which makes it possible to compute the effect of restricted diffusion efficiently and accurately. $E(\psi)$ is fitted to the curves predicted by the theory assuming a specific compartment shape anisotropy to extract compartment size. It should be noted that the assumption on compartment shape anisotropy is based on the observations of long-t_m measurements. In analyzing the data obtained from yeast cells, a spherical geometry was assumed based on the observations of d-PFG measurements with long mixing times (see below). In the phantom, such measurements indicated the presence of compartment shape anisotropy, and therefore an infinite cylinder model was employed. Based on the s-PFG measurements that yielded no EA, the cylinders were assumed to be randomly distributed. When there is a continuous distribution of cylinders, one needs to evaluate an integral over a sphere spanned by all orientations of the (infinitely long or capped) cylinders. This integral, which takes into account the orientational averaging of the cylinders, can be evaluated by employing an iterated Gaussian quadrature technique. In our implementation, we used such a scheme with 48 transformation points. A Levenberg–Marquardt algorithm was employed using the MPFIT package in IDL (provided at http://www.physics.wisc.edu/~craigm/idl/fitting.html). The uncertainty of each data point was assumed to be 1%, and the extracted values are reported as the mean ± standard deviation. A bicompartmental model (37) was fitted to the datasets from both specimens to account for the effects of a freely diffusing component, as the presence of Gaussian diffusion affects the signal decay along both the q axis and ψ axis (37). However, for the yeast cell dataset, different values for bulk diffusivity were allowed for the extracellular and intracellular spaces.

The $E(\psi)$ datasets from the yeast cells (but not the phantom, see below) were additionally fitted to Mitra's theory (29), so that the microstructural information obtained could be compared between a method that assumes the short gradient pulse approximation (29) and the new theory that takes the finite gradient lengths into account in the angular d-PFG experiments (32,33).

Experimental

Specimen preparation

Yeast cells. Approximately 1.5 g of commercially available dry *Saccharomyces cerevisiae* were hydrated with approximately 40 mL of phosphate-buffered saline. The mixture was vortexed for several minutes and subsequently centrifuged at 1000 rpm for 10 min. The supernatant fluid was decanted, and approximately 40 mL of 4% paraformaldehyde (Sigma-Aldrich, Rehovot, Israel) were added to the pellet. The yeast cells were vortexed, immersed in paraformaldehyde for 90 min and then centrifuged at 1200 rpm for 10 min. The supernatant was again removed, and the fixed cells were washed twice with phosphate-buffered saline and centrifuged at 1200 rpm. No bubbling or activity could be visually detected after fixation. Finally, the 0.6 g of fixed yeast pellet was hydrated with 800 μL of phosphate-buffered saline, vortexed and transferred to the NMR tube. The fixed yeast cells were allowed to settle in the NMR tube overnight at 4°C, and a small portion of fluid that collected on top of the yeast was aspirated prior to the NMR experiments.

Randomly oriented cylinders. The preparation of such controlled porous media has been described previously (42). Briefly, water-filled microcapillaries with a well-known inner diameter of 29 ± 1 μm were first cut to macroscopic ~5–10-mm-long pieces, which were briefly dried externally. Subsequently, these microtubes were crushed by mechanical force to very small dust-like particles which were re-immersed in water for several days for filling. The resulting porous medium was carefully dried externally and placed in an 8-mm NMR tube filled with Fluorinert. Owing to density and polarity differences between water and Fluorinert, any water residue on the outer portion of the crushed microcapillaries floated to the top of the NMR tube, outside the receiver coils, whereas the water within the inner diameter of the crushed microcapillaries was trapped in the intratubular space. Owing to their macroscopic small size, the pores assumed a completely random orientation whilst retaining their cylindrical geometry, with an inner diameter of approximately 29 ± 1 μm and axial dimension on the order of ~100–800 μm (42).

NMR experiments

The NMR experiments were conducted in an 8.4-T Bruker (Karlsruhe, Germany) NMR spectrometer, equipped with a Micro5 probe capable of producing nominal pulsed gradients up to 1900 mT/m in the x, y and z directions. The temperature was kept constant throughout the experiments at T = 303 K. All specimens were allowed to equilibrate with the magnet temperature for at least 1 h prior to the NMR experiments.

For both fixed yeast cells and phantom, the methodology of angular d-PFG MR experiments was performed as published previously (34,37,42). Briefly, $\mathbf{G_1}$ was set in the x direction, and the orientation of $\mathbf{G_2}$ was varied in the x–y plane along 25 different values of ψ (Fig. 2A). It should be noted that in these angular d-PFG experiments, the mixing time, diffusion and gradient magnitude are kept constant for each $E(\psi)$ profile. The only variant is the relative angle between the gradient vectors ψ. The magnitudes of the gradients are kept constant, e.g. $|\mathbf{G_1}| = |\mathbf{G_2}|$, resulting in $|\mathbf{q_1}| = |\mathbf{q_2}| = |\mathbf{q}|$ for each $E(\psi)$ profile.

Yeast cells. s-PFG experiments were performed using a stimulated echo sequence employing bipolar gradients. Experiments were performed in the x, y and z directions with the following parameters: 48 q values were collected with G_{max} = 1600 mT/m and Δ/δ = 200/3 ms, resulting in a q_{max} value of 2043 cm^{-1}.

Another s-PFG experiment (with conventional monopolar gradients) was performed for the q-space analysis with the

following parameters: 96 q values were collected with G_{max}=1600 mT/m and Δ/δ=50/2 ms, resulting in a q_{max} value of 1362 cm^{-1}.

The conventional angular d-PFG experiments were performed with the sequence shown in Fig. 1B, with the following parameters: eight q values were collected with G=25, 136, 246, 357, 468, 579, 689 and 800 mT/m with $\delta_1=\delta_2=\delta_3$=2 ms, resulting in q values of 21.3, 115.8, 209.4, 304, 398.5, 493, 586.5 and 681.3 cm^{-1}, respectively, and with $\Delta_1=\Delta_2$=250 ms and t_m=0 ms.

The bipolar d-PFG experiments were performed with the sequences shown in Fig. 1C, D. For t_m=0 ms, the sequence shown in Fig. 1D was used. Ten q values were collected with G=25, 111, 197, 283, 369, 456, 542, 628, 714 and 800 mT/m and $\delta_1=\delta_2=\delta_3$=3 ms, resulting in q values of 32, 141.8, 251.6, 361.5, 471.4, 582.5, 692.3, 802.2, 912 and 1021.9 cm^{-1}, respectively, and with $\Delta_1=\Delta_2$=200 ms. For the finite mixing time experiments, the sequence shown in Fig. 1C was used with exactly the same parameters, except $\delta_1=\delta_2$=3 ms, and t_m was set to 8.4, 11.4 and 19.4 ms.

Randomly oriented cylinders. The bipolar s-PFG sequence was performed in the x, y and z directions using the following parameters: 32 q values were collected with G_{max}=800 mT/m and Δ/δ=250/3 ms, resulting in q_{max}=1021.5 cm^{-1}.

The bipolar d-PFG experiments were performed with the sequences shown in Fig. 1C, D. For t_m=0 ms, the sequence shown in Fig. 1D was used. Seven q values were acquired with gradients of 25, 54, 83, 112, 142, 171 and 200 mT/m and with $\delta_1=\delta_2=\delta_3$=2.6 ms, resulting in q values of 27.6, 59.8, 91.9, 124, 157.2, 189.3 and 221.4 cm^{-1}, respectively, and with $\Delta_1=\Delta_2$=250 ms. For the finite mixing time experiments, the sequence shown in Fig. 1C was used with exactly the same parameters, except $\delta_1=\delta_2$=2.6 ms, and experiments with t_m of 7.6, 10.6, 18.6, 53.6 and 103.6 ms were acquired.

Light microscopy

The fixed yeast cells were taken from the NMR tube after the NMR experiments, diluted 1:50 in phosphate-buffered saline, and placed on a coverslip. To capture images of the fixed yeast cells, an Olympus IX71, Tokyo, Japan microscope was used with ×60 amplification.

Quantification of cellular size from microscopy images

Fifteen separate microscope images were imported to ImageJ software (National Institutes of Health, Bethesda, MD, USA; http://rsb.info.nih.gov/ij/) and a threshold was set such that cells were demarcated from their neighbors optimally. The Feret radius (longest distance within a domain) was automatically measured for approximately 900 cells. After inspection of the yeast cell size visually, Feret radii smaller than 3 μm or larger than 7 μm were excluded from the analysis as ImageJ analysis takes parts of cells or tends to clump cells together as one object, respectively. The histograms of the cells were then plotted, from which the mean cell size ± standard displacement was extracted. The analysis of the NMR results was completely blinded from the size extracted by microscopy.

Size extraction from s-PFG q-space experiment

The q-space analysis was performed only for the yeast cell specimen as, in the randomly oriented cylinder phantom, the analysis would be much less accurate owing to the lack of EA. The $E(q)$ data were Fourier transformed, affording the displacement PDF. The PDF was then fitted to a bi-Gaussian function, assuming one fast diffusing component and one slow diffusing component. The full width at half-maximum of each Gaussian was used to obtain the root-mean-square deviation of each component (15,16).

RESULTS

To determine whether diffusion in the yeast cell specimen is anisotropic (i.e. whether EA exists), we conducted bipolar s-PFG NMR experiments in the x, y and z directions. The bipolar gradients were used to ensure that susceptibility effects did not cause any directional preference. Figure 3A shows the data from these experiments. An isotropic signal decay was observed, suggesting that there is no EA present within the yeast cell specimen. However, this information is not sufficient to infer whether the cells are spherical or anisotropic but randomly oriented as in both cases, similar isotropic profiles will be obtained. Indeed, Fig. 3B shows a similar isotropic decay in the control phantom comprising randomly oriented water-filled cylindrical compartments having a nominal inner diameter of 29 ± 1 μm, demonstrating

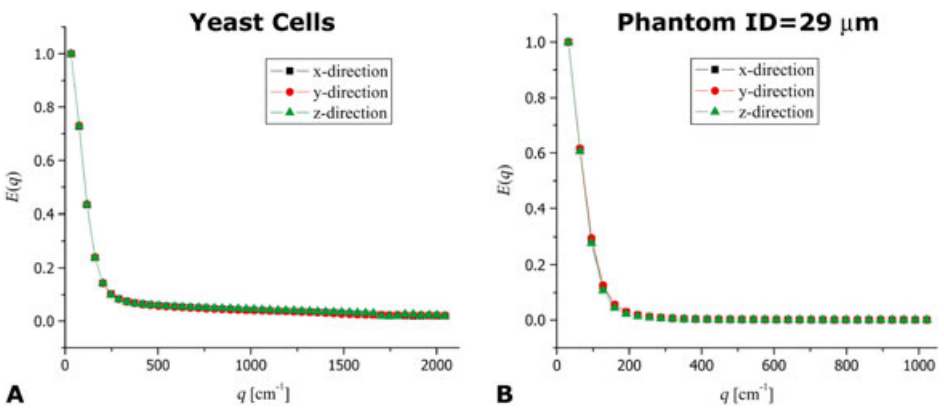

Figure 3. Bipolar single-pulsed field gradient (s-PFG) experiments in yeast cells and phantoms. (A) Bipolar s-PFG experiments conducted on fixed yeast cells with Δ=200 ms. The signal attenuation in the x, y and z directions is very similar, indicating the macroscopic isotropy of the cells. (B) Similar bipolar s-PFG experiments conducted on the phantom comprising randomly oriented cylinders having an inner diameter (ID) of 29 ± 1 μm with Δ=250 ms.

the limitation of s-PFG MR to distinguish between the two scenarios depicted in Fig. 2B and 2C.

To obtain further microstructural information on the local cellular shape, we performed angular bipolar d-PFG experiments with increasing t_m for both yeast cells and the control phantom (Fig. 4). The $E(\psi)$ profile from the yeast cells at $t_m=0$ ms and $2q=531\,cm^{-1}$ can be seen in Fig. 4A. An angular dependence in the form of a bell-shaped function can be readily observed, and the signal increases between $\psi=0°$ and $\psi=180°$ by about 10%, subsequently declining back to its original value at $\psi=360°$. It should be noted that the signal-to-noise ratio of the NMR signal in the yeast cells was more than 1000, even at the highest q values employed in this study. Importantly, this $E(\psi)$ angular dependence already bears important microstructural information: it unequivocally demonstrates the presence of μA, arising solely from restricted diffusion. However, to allow the effects of compartment shape anisotropy to become accentuated, long mixing times are needed (33). In fixed yeast cells, already at a relatively short value of $t_m=8.4$ ms, the angular profile becomes flat and remains flat for increasing values of t_m (Fig. 4A). Such a flat profile at long t_m is expected for spherical compartments and was observed for all q values (data not shown).

In the control phantom, however, where anisotropic compartments were randomly oriented, several interesting phenomena were observed. Figure 4B shows $E(\psi)$ plots for various mixing times at $2q=181\,cm^{-1}$ using the bipolar d-PFG sequences shown in Fig. 1C, D. At $t_m=0$ ms, the $E(\psi)$ profile was somewhat different from that at $t_m=0$ ms in yeast cells, with the bell-shaped curve exhibiting slight modulations (at higher q values, these modulations were much more pronounced; data not shown). Moreover, a very pronounced modulation in the $E(\psi)$ signal was observed for all nonzero values of t_m, showing a decrease between $E(\psi=0°)$ and $E(\psi=90°)$ of approximately 20% before subsequently rising back towards $E(\psi=180°)$. This behavior was then mirrored up to $\psi=360°$.

These results unambiguously demonstrate that although there is no EA in either yeast cells or phantom, the local anisotropy of the yeast cells is very low, whereas the pores in the synthetic porous phantom are, in fact, anisotropic, randomly oriented compartments. Thus, these long-t_m measurements offered insight into what geometrical model could be used in the compartment size analysis: the flat $E(\psi)$ dependence implied that a spherical model could be used to extract cellular size in yeast cells, whereas the modulated $E(\psi)$ in the control phantom implied that an infinite cylindrical model could be used for the synthetic phantom.

Figure 5 presents a representative light microscopy image, showing the morphology of the yeast cells. The microscopy images clearly revealed that the yeast cells were indeed mostly spherical, with negligible eccentricity, validating the noninvasive long-t_m angular d-PFG MR results. Figure 5B shows the quantification of the yeast cell size. The average±standard deviation cellular size measured was 5.32±0.83 μm.

Figure 6A shows the $E(\psi)$ data from an angular d-PFG experiment at $t_m=0$ ms (symbols) for fixed yeast cells at three different q values, together with the fit to the theory (full lines). Clearly, the theoretical fit to the experimental data shows remarkable correspondence. It should be noted that the plateau-like feature that can be seen in the experimental data at higher q values is a susceptibility artifact that was corrected when bipolar gradients were used (data not shown). The size that was extracted from the fitting of the theory to the experimental angular d-PFG data was 5.46±0.45 μm ($R^2=0.979$). Moreover, when angular bipolar d-PFG measurements, in which the violation of the short gradient pulse approximation is more pronounced, were performed on yeast cells with $t_m=0$ ms, the size that was extracted using the general framework in refs. (32,33) did not vary significantly, and was found to be 5.37±0.22 μm ($R^2=0.999$). It should be noted that the datasets were analyzed completely blind, with no *a priori* knowledge of compartment size or even of the expected length scales within the specimen.

We also applied Mitra's theory (29) to extract the compartment size. The cellular size that was extracted using this approach in the angular d-PFG experiments was 4.31±0.06 μm, or about 20% lower than the size measured by microscopy. When Mitra's theory was employed to extract the compartment size from the bipolar d-PFG dataset, a much smaller size of 3.23± 0.04 μm was obtained, more than 40% smaller than the size measured by microscopy.

Figure 6B shows the $E(\psi)$ plots obtained from angular bipolar d-PFG at $t_m=0$ ms for three q values in the randomly oriented cylinders. Here, bipolar gradients are imperative for the compensation of severe susceptibility effects in the specimen (37). The symbols represent the experimental data and the full curves

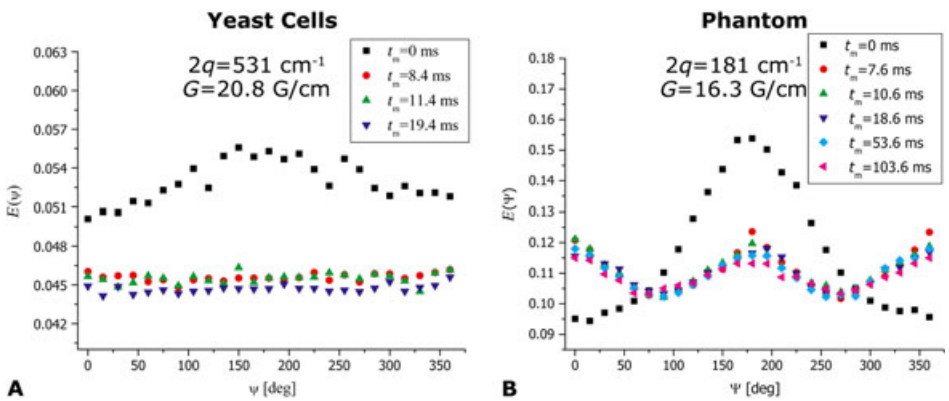

Figure 4. Bipolar double-pulsed field gradient (d-PFG) experiments depicting the mixing time dependence in yeast cells and in the phantom. (A) Bipolar d-PFG experiments in yeast cells showing that with increasing mixing time, a flat angular dependence is observed, conveying the spherical morphology of the cells. (B) Bipolar d-PFG conducted in the phantom with randomly oriented cylindrical compartments with an inner diameter (ID) of 29±1 μm. A qualitatively different t_m dependence can be seen, from which it can be inferred that the compartments are anisotropic, despite being completely randomly oriented. Note the pronounced modulations in $E(\psi)$ arising from compartment shape anisotropy.

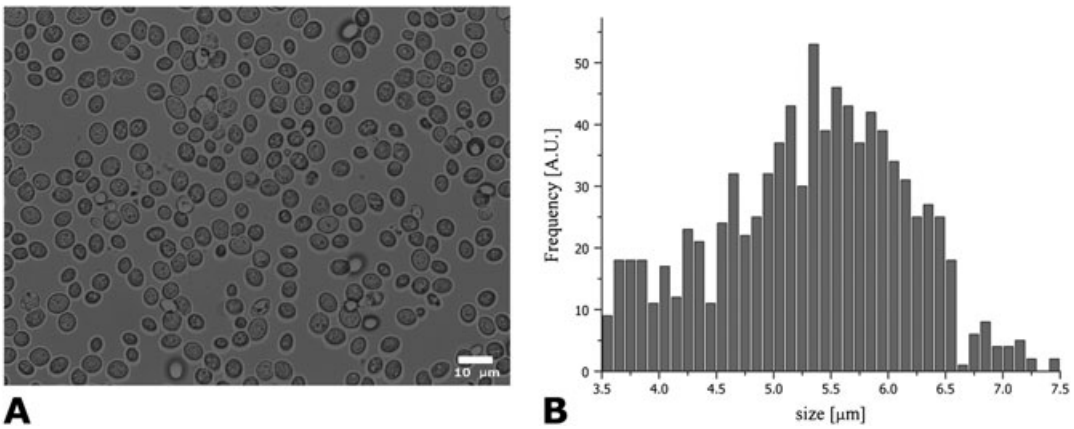

Figure 5. Microscopy and quantification of cell size. (A) Representative light microscopy image showing that the majority of cells are indeed relatively spherical. (B) Quantification of ~900 individual yeast cells resulted in a cell size of 5.32±0.83 μm.

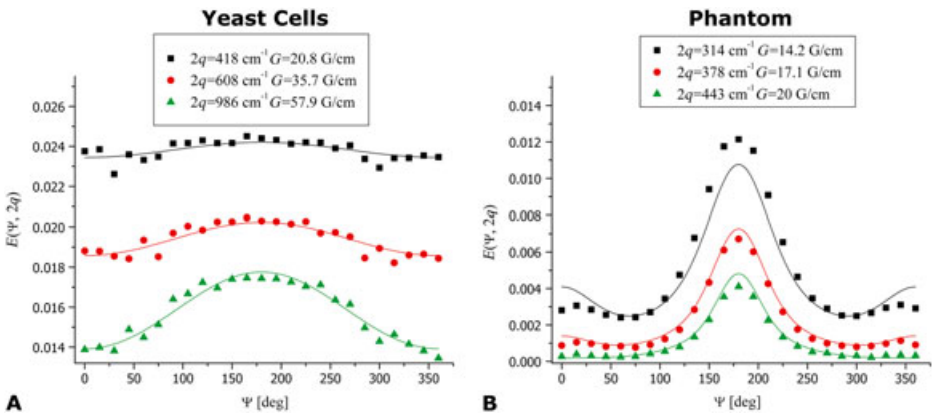

Figure 6. Quantification of cell size from noninvasive angular double-pulsed field gradient (d-PFG) MR. (A) d-PFG experiments (symbols) and theoretical fits (lines) in yeast cells show excellent agreement. The compartment size was extracted blind and was found to be 5.46±0.45 μm. (B) Bipolar d-PFG experiments (symbols) and theoretical fits (lines) in the phantom with an inner diameter (ID) of 29±1 μm. The size extracted was 27.08±0.22 μm, in good agreement with the nominal ID. The slight deviation from the nominal ID is probably a result of incomplete suppression of background gradients.

represent the fits to the theory. Based on the pronounced $E(\psi)$ modulation in Fig. 4B at long t_m, we used the infinite cylinder model for this specimen. The size that was extracted for the phantom was 27.06±0.22 μm (R^2=0.926), in good agreement with the nominal inner diameter.

To compare the d-PFG size measurements with the microstructural information that can be obtained using conventional s-PFG methods, a *q*-space experiment (12,13) was performed on the yeast cell specimen. The displacement PDF obtained from the Fourier transform of $E(q)$ was fitted to a bi-Gaussian function, and two components were extracted (15,16). The root-mean-square displacement of the slow component was 3.85±0.15 μm. Again, the size extracted is smaller than the nominal cell size measured from the invasive microscopy images.

DISCUSSION

Accurate measurements of morphological features, such as compartment size and shape, are desirable in many areas of research that require a 'fingerprint' of an optically turbid specimen. In biological applications, cell size and shape are of great significance for the characterization of cellular processes (9,48) in order to delineate different healthy (19,20) and diseased (49,50) regions owing to size contrast.

To determine the compartment dimensions, most applications use conventional s-PFG approaches ranging from diffusion–diffraction (6) or *q*-space MR (12,13) to more sophisticated methods for the determination of length scales (5,51–53). However, among the inherent limitations of the diffusion–diffraction approaches is that an *a priori* knowledge of the pore shape is needed to obtain accurate sizes (54); furthermore, when *q*-space approaches are used to obtain the root-mean-square displacement, the information on pore shape will not be available unless EA exists. In addition, the demand for very strong gradient amplitudes poses both a technological constraint (as it is currently relatively difficult to manufacture three-dimensional strong gradient systems) as well as a methodological limitation (as the signal-to-noise ratio at very high *q* values tends to be low). Finally, in many instances in biophysical applications, the diffusion modes within the specimen are hard to infer: for example, the assignment of water to intra-/extracellular spaces is controversial in many tissues in the central nervous system (55,56).

Previous studies on angular d-PFG MR, which is emerging as a valuable means for obtaining novel microstructural information

in settings in which conventional s-PFG methods are limited (i.e. when there is no coherent organization of compartments), have mainly focused on validating the methodology and challenging the microstructural information that can be obtained from well-controlled phantoms, where an *a priori* knowledge of the ground truth is a major advantage (34,37,42–44). Based on the foundations laid by the former studies in controlled specimens, we applied the angular d-PFG methodology in yeast cells, and also in another phantom in which no EA exists. It should be noted that yeast cells were also the substrate of the first published d-PFG study, which employed high-q-value d-PFG measurements to infer the eccentricity of irradiated yeast cells (22). Further studies in yeast cells (23) and liquid crystals (24) demonstrated that information on locally anisotropic motions within randomly oriented specimens could indeed be inferred from a comparison of $E(q)$ signal decays (up to high q values) in collinear and orthogonal (nonangular) d-PFG MR.

The main goals of this study were to measure accurate compartment size in yeast cells and to infer additional morphological information that could be obtained on compartment eccentricity. Before one can attempt to extract accurate cellular size, some knowledge of the underlying anisotropy of the cells and their organization needs to be determined so that a suitable model can be selected for size analysis. As, macroscopically, both yeast cells and randomly oriented cylinders exhibit isotropic diffusion, the bipolar s-PFG experiments yielded isotropic signal decay, demonstrating that bipolar s-PFG experiments could not distinguish between these diffusion scenarios, for which EA is not present. Angular d-PFG MR, however, can manifest the effects of anisotropy on a microscopic scale owing to restriction (μA), which can be used to infer the compartment size, as well as the effects of compartment shape anisotropy that arise from compartment eccentricity, even at low q values. Therefore, angular d-PFG MR has the potential to report on the compartment size and compartment shape anisotropy.

Although the bipolar s-PFG MR experiments did not report on the underlying microstructure, we demonstrated here, for the first time, that $E(\psi)$ plots at long t_m in angular bipolar d-PFG experiments provide shape contrast between spherical yeast cells and randomly oriented cylindrical compartments based on their respective compartment eccentricity: the spherical cells exhibited a ψ-independent angular dependence at long t_m, whereas the randomly oriented cylinders exhibited a marked modulation of the $E(\psi)$ plots, both phenomena predicted by theory (33). It should be noted that, although one can infer compartment shape anisotropy when $E(\psi)$ curves appear modulated and estimates for compartment eccentricity can be obtained (33), it is practically not possible to distinguish between compartments having similar eccentricities but different shapes, such as ellipsoids and capped cylinders. This means that the fine details of the geometry would be difficult to resolve in angular d-PFG NMR at long t_m. However, although the exact shape of the pore cannot be measured, the shape anisotropy is available from long-t_m angular d-PFG NMR. Such estimates of the eccentricity of the compartments represent important microstructural information that is unavailable from s-PFG MR. It seems, therefore, that the angular d-PFG MR methodology offers novel microstructural information on the underlying compartment morphology.

Although the modulation in the $E(\psi)$ curve owing to compartment shape anisotropy at long t_m has been shown recently for the first time (42), in this study, we also investigated the t_m dependence in a sequence that employed z storage of magnetization during most of the mixing time. Such t_m-dependent measurements could be important, especially when there is a distribution of length scales, to ensure that μA has been completely decoupled, albeit not introducing further T_2 weighting with increasing t_m. Interestingly, we found that even relatively short t_m is sufficient to decouple μA from compartment shape anisotropy, even in relatively large compartments, when bipolar d-PFG is used, probably owing to the effective mixing time that is induced in the bipolar d-PFG sequence during the time between the split gradients. It should be noted that it is possible to attempt to extract compartment size even in the long-t_m regime; however, as the information on μA is lost at long t_m and a ψ-independent curve is obtained for the yeast cells, the fitting would amount to no more than fitting multiple, but identical, $E(q)$ profiles; therefore, the useful additional dimension that is provided by the angle ψ to infer on μA is not fully exploited.

Once the compartment shape anisotropy has been determined noninvasively, one can then use the theory to accurately measure compartment size employing angular d-PFG MR at relatively low q values. It should be noted that long-t_m angular d-PFG MR experiments provide an indication of what model can be used to analyze the short-t_m experiments in terms of compartment anisotropy. In yeast cells, the ψ-independent curves at long t_m justified the use of a spherical model to fit the data. The correspondence between the cell size obtained by noninvasive spectroscopy and invasive light microscopy is striking. Importantly, and of potential clinical relevance, is that the sizes were robustly extracted at low q values, comparable with the q values in which diffusion tensor imaging is routinely performed, and using relatively weak gradients, albeit not as weak as currently allowed in the clinic. An increase of up to approximately 10% was demonstrated here in the signal arising from angular d-PFG experiments using gradient strengths of only 208 mT/m, from which the accurate size (5.46 ± 0.45 μm) could be extracted, much lower than the gradients needed to perform s-PFG q-space MR or the gradients previously used to measure the eccentricity of yeast cells (23). In the phantom, the modulated $E(\psi)$ plots at long t_m implied that the pores are anisotropic, albeit being randomly oriented. When an infinite cylinder shape was assumed for the pores in the phantom, the size extracted from angular bipolar d-PFG measurements was also in very good agreement with the nominal inner diameter of 29 ± 1 μm, and the slight deviation from the nominal diameter can be attributed to incomplete suppression of the background gradient, despite the use of bipolar gradients (note that the linewidth in these specimens was very broad, around ~500 Hz). Another factor that may contribute to the slight deviation is that a temporally dependent background gradient may emerge, further complicating the cross terms between diffusion and background gradients (57). We also attempted a fit using a capped cylinder shape assumption (data not shown), and the results yielded a diameter of 27.04 ± 0.96 μm and a length of 530.26 ± 97.99 μm. Indeed, these results imply that the length/radius ratio is very large and justifies the use of infinite cylinders. It should be noted that the diffusion time (250 ms) was not sufficiently long to probe restriction on a length scale of ~500 μm, again indicating that an infinite model should be used.

The $E(\psi)$ plots at $t_m = 0$ ms also provide insight into the prevailing diffusion modes in the specimens. When restricted, non-Gaussian diffusion is the only prevalent diffusion mode in the specimen, the $E(\psi)$ bell-shaped dependences should be

detectable at low q values. However, in a previous study, a controlled bicompartmental phantom (37) was used to study the effect of a freely diffusing component on the $E(\psi)$ plots. In that phantom, restricted diffusion arising from water confined in microcapillaries was superimposed with freely diffusing water. There, it was shown that at low q values, free diffusion masks the bell-shaped functions arising from restricted diffusion in the coherently placed cylinders, yielding flat $E(\psi)$ profiles; however, the bell shape in $E(\psi)$ reappeared at slightly higher q values, when free diffusion was suppressed (37). As the free diffusion term in the signal decay is Δ dependent, prolonging Δ suppressed the fast component at lower q values, and the $E(\psi)$ dependences arising from the restricted component could therefore be emphasized at these lower q values (37). Interestingly, in the yeast cell specimen, the angular dependence was relatively flat up to $2q \sim 400\,\mathrm{cm}^{-1}$ (data not shown) and the bell-shaped dependences emerged at slightly higher q values. As in the bicompartmental phantom, this low-q behavior was also diffusion time dependent (data not shown), leading to the conclusion that indeed, the low-q part of the signal is dominated by the attenuation arising from Gaussian diffusion, whereas at slightly higher q values, the free component is largely suppressed, accentuating the restricted component (37). As the size measurement appears to be in excellent correspondence with the cellular size obtained from microscopy, it seems that the bell-shaped functions arise mostly from the intracellular space. Therefore, it seems reasonable to infer that the freely diffusing Gaussian component in the yeast specimen arises from extracellular diffusion. This distinction may become important in other cellular environments, such as central nervous system tissues, where diffusion in the extracellular space may exhibit hindered or even restricted attributes. In this study, the effects of exchange were not considered, as there is yet no theory on exchange effects in angular d-PFG MR. However, it seems that, owing to the remarkable agreement between the extracted cell diameter and the spectroscopy measurements, together with the observation that cells are spherical, exchange effects are not very significant in this experimental set-up.

It should be noted that, in the q-space analysis, for example, the PDFs generated from the Fourier transform of $E(q)$ data can be fitted to a bi-Gaussian function. This analysis, which is equivalent to fitting a bi-Gaussian function to the $E(q)$ data [or similar to fitting a bi-exponential to the $E(b)$ data], assumes that the reconstructed propagator is truly bi-Gaussian, with different Gaussians representing different geometric compartments. Therefore, the q-space approach differs from the method employed to analyze the d-PFG data in that diffusion in the intracellular space is assumed to be Gaussian as well. Considering that the maximum q value in s-PFG acquisitions was $1362\,\mathrm{cm}^{-1}$ in this study, the $2\pi qa$ value, with a compartment size of $a \sim 4\,\mu\mathrm{m}$, is greater than unity. Therefore, for a wide range of q values, the Gaussian assumption is expected to hold when $2\pi qa < 1$ is less accurate. Despite this shortcoming of the approach, the value obtained from the analysis is in reasonable proximity to the expected value, and it is possible to attribute the deviation towards smaller sizes to the violation of the short gradient pulse approximation or to the truncation of the $E(q)$ plots at $q = 1362\,\mathrm{cm}^{-1}$. It should be noted that the q-space analysis was not performed for the randomly oriented cylinders owing to their distribution of lengths and orientational dispersion.

Several groups have employed angular d-PFG in imaging using Mitra's theory (29) to extract compartment sizes (35,36), despite violating the theory's limiting conditions. When Mitra's theory was used to extract the cell size, significant deviations from the nominal size were obtained owing to the violation of Mitra's limiting conditions (29). This is consistent with previous experimental findings on controlled phantoms (34), as well as with others' simulations (36,40). This deviation is expected to become more pronounced in smaller compartments; therefore, using theoretical frameworks that take into account every experimental parameter is clearly beneficial. We did not attempt to fit the randomly oriented cylinders using Mitra's framework, as, for an arbitrary orientation of the cylinder, the components of the two gradients perpendicular to the cylinder would not be equal to one another, thus violating Mitra's $G_1 = G_2$ assumption (29). This was not an issue in ref. (34) because there, both gradients had been applied perpendicular to the walls of coherently oriented cylinders, and all experiments had employed gradients of equal strength.

CONCLUSIONS

To conclude, systems in which no EA exists were investigated using conventional s-PFG NMR and angular d-PFG NMR that was conducted using weak gradients. Accurate cellular size and shape anisotropy were measured at low q values from angular d-PFG experiments in fixed yeast cells. The spherical shape of the cells was inferred at long mixing times, obviating the need to assume a priori the compartment shape, and the sizes were extracted from experiments with $t_m = 0\,\mathrm{ms}$, which also conveys μA in the specimen. The correspondence of the extracted cellular sizes with invasive microscopy demonstrated that the size and shape measurements were indeed accurate. These findings are promising for application of d-PFG MR in other heterogeneous systems (58,59) as well as in d-PFG MRI, for example.

Acknowledgements

P.J.B, and E.Ö. were supported by the Intramural Research Program of the Eunice Kennedy Shriver National Institute of Child Health and Human Development, National Institutes of Health (NIH), Department of Defense in the Center for Neurosciences and Regenerative Medicine (CNRM) and the Henry M. Jackson Foundation (HJF). Y.C., N.S., E.Ö.and P.J.B. were partially supported by a grant from the US-Israel Binational Foundation (BSF, grant number 2009155). N.S. would like to gratefully acknowledge the Clore Scholar's Program for a scholarship. The authors acknowledge Dr Yael Roichman and Ms. Tal Maya from the School of Chemistry at Tel Aviv University for their assistance with light microscopy.

REFERENCES

1. Stejskal EO, Tanner JE. Spin diffusion measurements – spin echoes in presence of a time-dependent field gradient. J. Chem. Phys. 1965; 42: 288–292.
2. Basser PJ, Mattiello J, Lebihan D. Diffusion tensor spectroscopy and imaging. Biophys. J. 1994; 66: 259–267.
3. Regan DG, Kuchel PW. Simulations of molecular diffusion in lattices of cells: insights for NMR of red blood cells. Biophys. J. 2002; 83: 161–171.
4. Kuntz JF, Trausch G, Palmas P, Mutzenhardt P, Canet D. Diffusive diffraction phenomenon in a porous polymer material observed by NMR using radio-frequency field gradients. J. Chem. Phys. 2007; 126: 134904 (1–6).

5. Song YQ, Ryu SG, Sen PN. Determining multiple length scales in rocks. Nature 2000; 406: 178–181.
6. Callaghan PT, Coy A, Macgowan D, Packer KJ, Zelaya FO. Diffraction-like effects in NMR diffusion studies of fluids in porous solids. Nature 1991; 351: 467–469.
7. Avram L, Assaf Y, Cohen Y. The effect of rotational angle and experimental parameters on the diffraction patterns and micro-structural information obtained from q-space diffusion NMR: implication for diffusion in white matter fibers. J. Magn. Reson. 2004; 169: 30–38.
8. Kuchel PW, Coy A, Stilbs P. NMR 'diffusion–diffraction' of water revealing alignment of erythrocytes in a magnetic field and their dimensions and membrane transport characteristics. Magn. Reson. Med. 1997; 37: 637–643.
9. Pages G, Szekely D, Kuchel PW. Erythrocyte-shape evolution recorded with fast-measurement NMR diffusion–diffraction. J. Magn. Reson. Imaging 2008; 28: 1409–1416.
10. Topgaard D, Malmborg C, Söderman O. Restricted self-diffusion of water in a highly concentrated W/O emulsion studied using modulated gradient spin-echo NMR. J. Magn. Reson. 2002; 156: 195–201.
11. Feintuch A, Grayevsky A, Kaplan N, Dormann E. Diffusive diffraction of the local ESR pulse-gradient spin-echo signal in a restricted one-dimensional conductor. Phys. Rev. Lett. 2004; 92: 156803 (1–4).
12. Cory DG, Garroway AN. Measurement of translational displacement probabilities by NMR – an indicator of compartmentation. Magn. Reson. Med. 1990; 14: 435–444.
13. Cohen Y, Assaf Y. High b-value q-space analyzed diffusion-weighted MRS and MRI in neuronal tissues – a technical review. NMR Biomed. 2002; 15: 516–542.
14. Assaf Y, Mayk A, Cohen Y. Displacement imaging of spinal cord using q-space diffusion-weighted MRI. Magn. Reson. Med. 2000; 44: 713–722.
15. Bar-Shir A, Cohen Y. High b-value q-space diffusion MRS of nerves: structural information and comparison with histological evidence. NMR Biomed. 2008; 21: 165–174.
16. Bar-Shir A, Duncan ID, Cohen Y. QSI and DTI of excised brains of the myelin-deficient rat. Neuroimage 2009; 48: 109–116.
17. Biton IE, Duncan ID, Cohen Y. q-space diffusion of myelin-deficient spinal cords. Magn. Reson. Med. 2007; 58: 993–1000.
18. King MD, Houseman J, Roussel SA, Vanbruggen N, Williams SR, Gadian DG. Q-space imaging of the brain. Magn. Reson. Med. 1994; 32: 707–713.
19. Ong HH, Wright AC, Wehrli SL, Souza A, Schwartz ED, Hwang SN, Wehrli FW. Indirect measurement of regional axon diameter in excised mouse spinal cord with q-space imaging: simulation and experimental studies. Neuroimage 2008; 40: 1619–1632.
20. Ong HH, Wehrli FW. Quantifying axon diameter and intra-cellular volume fraction in excised mouse spinal cord with q-space imaging. Neuroimage 2010; 51: 1360–1366.
21. Johansen-Berg H, Behrens TEJ (eds). *Diffusion MRI: From Quantitative Measurement to In-Vivo Neuroanatomy*. Academic Press: London, UK; 2009.
22. Cory DG, Garroway AN, Miller JB. Applications of spin transport as a probe of local geometry. Polym. Prepr. 1990; 31: 149–150.
23. Cheng Y, Cory DG. Multiple scattering by NMR. J. Am. Chem. Soc. 1999; 121: 7935–7936.
24. Callaghan PT, Komlosh ME. Locally anisotropic motion in a macroscopically isotropic system: displacement correlations measured using double pulsed gradient spin-echo NMR. Magn. Reson. Chem. 2002; 40: S15–S19.
25. Komlosh ME, Horkay F, Freldlin RZ, Nevo U, Assaf Y, Basser PJ. Detection of microscopic anisotropy in gray matter and in a novel tissue phantom using double pulsed gradient spin echo MR. J. Magn. Reson. 2007; 189: 38–45.
26. Komlosh ME, Lizak MJ, Horkay F, Freidlin RZ, Basser PJ. Observation of microscopic diffusion anisotropy in the spinal cord using double-pulsed gradient spin echo MRI. Magn. Reson. Med. 2008; 59: 803–809.
27. Blumich B, Callaghan PT, Damion RA, Han S, Khrapitchev AA, Packer KJ, Stapf S. Two-dimensional NMR of velocity exchange: VEXSY and SERPENT. J. Magn. Reson. 2001; 152: 162–167.
28. Callaghan PT, Godefroy S, Ryland BN. Use of the second dimension in PGSE NMR studies of porous media. Magn. Reson. Imaging 2003; 21: 243–248.
29. Mitra PP. Multiple wave-vector extensions of the NMR Pulsed-field-gradient spin-echo diffusion measurement. Phys. Rev. B 1995; 51: 15074–15078.
30. Özarslan E, Basser PJ. MR diffusion–'diffraction' phenomenon in multi-pulse-field-gradient experiments. J. Magn. Reson. 2007; 188: 285–294.
31. Özarslan E, Basser PJ. Microscopic anisotropy revealed by NMR double pulsed field gradient experiments with arbitrary timing parameters. J. Chem. Phys. 2008; 128: 154511 (1–11).
32. Özarslan E, Shemesh N, Basser PJ. A general framework to quantify the effect of restricted diffusion on the NMR signal with applications to double pulsed field gradient NMR experiments. J. Chem. Phys. 2009; 130: 104702 (1–9).
33. Özarslan E. Compartment shape anisotropy (CSA) revealed by double pulsed field gradient MR. J. Magn. Reson. 2009; 199: 56–67.
34. Shemesh N, Özarslan E, Basser PJ, Cohen Y. Measuring small compartmental dimensions with low-q angular double-PGSE NMR: the effect of experimental parameters on signal decay. J. Magn. Reson. 2009; 198: 15–23.
35. Koch MA, Finsterbusch J. Compartment size estimation with double wave vector diffusion-weighted imaging. Magn. Reson. Med. 2008; 60: 90–101.
36. Weber T, Ziener CH, Kampf T, Herold V, Bauer WR, Jakob PM. Measurement of apparent cell radii using a multiple wave vector diffusion experiment. Magn. Reson. Med. 2009; 61: 1001–1006.
37. Shemesh N, Özarslan E, Bar-Shir A, Basser PJ, Cohen Y. Observation of restricted diffusion in the presence of a free diffusion compartment: single- and double-PFG experiments. J. Magn. Reson. 2009; 200: 214–225.
38. Finsterbusch J, Koch MA. A tensor approach to double wave vector diffusion-weighting experiments on restricted diffusion. J. Magn. Reson. 2008; 195: 23–32.
39. Finsterbusch J. Extension of the double-wave-vector diffusion-weighting experiment to multiple concatenations. J. Magn. Reson. 2009; 198: 174–182.
40. Koch MA, Finsterbusch J. Numerical simulation of double-wave vector experiments investigating diffusion in randomly oriented ellipsoidal pores. Magn. Reson. Med. 2009; 62: 247–254.
41. Lawrenz M, Koch MA, Finsterbusch J. A tensor model and measures of microscopic anisotropy for double-wave-vector diffusion-weighting experiments with long mixing times. J. Magn. Reson. 2009; 202: 43–56.
42. Shemesh N, Özarslan E, Adiri T, Basser PJ, Cohen Y. Noninvasive bipolar double-pulsed-field-gradient NMR reveals signatures for pore size and shape in randomly oriented, polydisperse, inhomogeneous porous media. J. Chem. Phys. 2010; 133: 044705(1–9).
43. Shemesh N, Cohen Y. The effect of experimental parameters on the signal decay in double-PGSE experiments: negative diffractions and enhancement of structural information. J. Magn. Reson. 2008; 195: 153–161.
44. Shemesh N, Özarslan E, Basser PJ, Cohen Y. Detecting diffusion–diffraction patterns in size distribution phantoms using double-pulsed field gradient (d-PFG) NMR: theory and experiments. J. Chem. Phys. 2010; 132: 034703 (1–12).
45. Aslund I, Topgaard D. Determination of the self-diffusion coefficient of intracellular water using PGSE NMR with variable gradient pulse length. J. Magn. Reson. 2009; 201: 250–254.
46. Aslund I, Nowacka A, Nilsson M, Topgaard D. Filter-exchange PGSE NMR determination of cell membrane permeability. J. Magn. Reson. 2009; 200: 291–295.
47. Malmborg C, Sjobeck M, Brockstedt S, Englund E, Söderman O, Topgaard D. Mapping the intracellular fraction of water by varying the gradient pulse length in q-space diffusion MRI. J. Magn. Reson. 2006; 180: 280–285.
48. Torres AM, Michniewicz RJ, Chapman BE, Young GAR, Kuchel PW. Characterisation of erythrocyte shapes and sizes by NMR diffusion–diffraction of water: correlations with electron micrographs. Magn. Reson. Imaging 1998; 16: 423–434.
49. Assaf Y, Ben-Bashat D, Chapman J, Peled S, Biton IE, Kafri M, Segev Y, Hendler T, Korczyn AD, Graif M, Cohen Y. High b-value q-space analyzed diffusion-weighted MRI: application to multiple sclerosis. Magn. Reson. Med. 2002; 47: 115–126.
50. Biton IE, Mayk A, Kidron D, Assaf Y, Cohen Y. Improved detectability of experimental allergic encephalomyelitis in excised swine spinal cords by high b-value q-space DWI. Exp. Neurol. 2005; 195: 437–446.
51. Assaf Y, Basser PJ. Composite hindered and restricted model of diffusion (CHARMED) MR imaging of the human brain. Neuroimage 2005; 27:

52. Assaf Y, Blumenfeld-Katzir T, Yovel Y, Basser PJ. AxCaliber: a method for measuring axon diameter distribution from diffusion MRI. Magn. Reson. Med. 2008; 59: 1347–1354.
53. Drobnjak I., Siow B, Alexander DC. Optimizing gradient waveforms for microstructure sensitivity in diffusion-weighted MR. J. Magn. Reson. 2010; 206: 41–51.
54. Codd SL, Callaghan PT. Spin echo analysis of restricted diffusion under generalized gradient waveforms: planar, cylindrical, and spherical pores with wall relaxivity. J. Magn. Reson. 1999; 137: 358–372.
55. Beaulieu C. The basis of anisotropic water diffusion in the nervous system – a technical review. NMR Biomed. 2002; 15: 435–455.
56. Clark CA, Le Bihan D. Water diffusion compartmentation and anisotropy at high b values in the human brain. Magn. Reson. Med. 2000; 44: 852–859.
57. Sun PZ, Seland JG, Cory D. Background gradient suppression in pulsed gradient stimulated echo measurements. J. Magn. Reson. 2003; 161: 168–173.
58. Shemesh N, Adiri T, Cohen Y. Probing microscopic architecture of opaque heterogeneous systems using double-Pulsed-Field-Gradient NMR. J. Am. Chem. Soc. 2011; 133: 6028–6035.
59. Shemesh N and Cohen Y. Microscopic and compartment shape anisotropies in gray and white matte revealed by angular bipolar d-PFG MR. Magn. Reson. Med. 2011; 65: 1216–1227.